MULTICRITERIA ANALYSIS OF AN L_1 ADAPTIVE FLIGHT CONTROL SYSTEM

Vladimir Dobrokhodov[1], Isaac Kaminer.[2]
Naval Postgraduate School, Monterey, CA 93943

Enric Xargay[3], Naira Hovakimyan[4]

University of Illinois at Urbana-Champaign, Urbana, IL 61801

Chengyu Cao[5]

University of Connecticut, Storrs, CT 06269

Irene M. Gregory[6]
NASA Langley Research Center, Hampton, VA 23681

This paper presents an overview of the application of the Parameter Space Investigation method for the multi-criteria design optimization of the $\mathcal{L}_1$ adaptive flight control system implemented on the two turbine-powered dynamically-scaled GTM AirSTAR aircraft. In particular, the study addresses the improvement of a nominal *prototype* solution, obtained using basic design guidelines of $\mathcal{L}_1$ adaptive control theory. The results validate the theoretical claims of $\mathcal{L}_1$ adaptive control in terms of closed-loop performance and robustness, and illustrate the systematic character of its design procedure. Furthermore, the paper shows the suitability of the Parameter Space Investigation method for the multi-criteria design optimization over a multi-dimensional design variable space of a flight control system subject to desired control specifications. The use of this particular method is of special interest, as it provides invaluable information about the behavior of the closed-loop system in an extended space of design parameters and performance criteria. The results and conclusions of this paper have led to a deeper understanding of the characteristics of the

[1] Associate Professor, Mechanical and Aerospace Engineering dept, vldobr@nps.edu.
[2] Professor, Mechanical and Aerospace Engineering dept, kaminer@nps.edu.
[3] Doctoral Student, Department of Aerospace Engineering, xargay@illinois.edu.
[4] Professor, Department of Aerospace Engineering, nhovakim@illinois.edu.
[5] Assistant Professor, Department of Mechanical Engineering ccao@engr.uconn.edu .
[6] Senior Aerospace Research Engineer, Dynamics Systems and Control Branch, MS 308, irene.m.gregory@nasa.gov .

closed-loop adaptive system, and have contributed to the improvement of the flying qualities and the robustness margins of the adaptive $\mathcal{L}_1$-augmented aircraft, which has been recently flight tested by NASA.

Key Words: $\mathcal{L}_1$ adaptive control, flying qualities, multi-criteria optimization, Pareto space, randomized algorithms.

I. Introduction

Adaptive control has long been seen as an appealing technology to improve aircraft performance with reduced pilot compensation in adverse flight conditions or in the event of control surface failures and vehicle damage. Under these conditions, which are characterized by a high degree of uncertainty with respect to a nominal aircraft, the achievable levels of performance and flying qualities (FQ) that a non-adaptive flight control system (FCS) can provide might be limited. However, several limitations of the conventional adaptive systems have prevented this technology from being widely used in safety-critical aerospace applications [1–3]. In particular, the key deficiencies of conventional adaptive (flight) control systems can be summarized as: (*i*) the lack of transient characterization of the closed-loop response; (*ii*) the limited framework for analysis of the robustness and performance properties of closed-loop adaptive systems; and *(iii)* the lack of systematic design guidelines to solve the tradeoff between adaptation, performance, and robustness.

The theory of $\mathcal{L}_1$ adaptive control overcomes the limitations of conventional adaptive control architectures described above, and enables the design of robust adaptive control architectures using fast adaptation schemes [4]. The key feature of $\mathcal{L}_1$ adaptive control is the decoupling of the adaptation loop from the control loop, which enables fast adaptation without sacrificing robustness. In fact, in $\mathcal{L}_1$ adaptive control architectures, the rate of the adaptation loop can be set arbitrarily high, subject only to hardware limitations (computational power and high-frequency sensor noise), while the tradeoff between performance and robustness can be addressed via conventional methods from classical and robust control. Fast adaptation enables compensation for the undesirable effects of rapidly varying uncertainties and

significant changes in system dynamics, and is thus critical towards achieving guaranteed transient performance without enforcing persistency of excitation or resorting to high-gain feedback. Moreover, the $\mathcal{L}_1$ adaptive control theory provides systematic design guidelines that significantly reduce the tuning effort of the adaptive controller.

The main challenge for the design of $\mathcal{L}_1$ FCSs is the optimal tuning of its elements to provide desired FQ with satisfactory robustness margins over large operational envelopes and uncertainty scenarios. While the theory of $\mathcal{L}_1$ adaptive control provides systematic design guidelines to address the tradeoff between performance and robustness, optimization of the design of $\mathcal{L}_1$ adaptive controllers is still largely open and hard to address. The main difficulty is the non-convex and non-smooth nature of the underlying optimization problem that involves the $\mathcal{L}_1$-norm of cascaded linear systems. Randomized parametric algorithms have been proven to be effective in control-related non-convex optimization problems, and therefore they seem attractive for the optimal design of $\mathcal{L}_1$ adaptive controllers [4],[5]. In particular, one of the approaches that can help to solve this multi-objective optimization problem is the Parameter Space Investigation (PSI) method [6], [7]. This method explicitly addresses the issues with high dimensionality of the design variable space, functional constraint space, and criteria space, and is implemented in a user-friendly and "model agnostic" software package called Multicriteria Optimization and Vector Identification (MOVI) [8].

In this paper, we take advantage of the systematic design guidelines of $\mathcal{L}_1$ adaptive control for the design optimization of the $\mathcal{L}_1$ FCS implemented on the Generic Transport Model (GTM), which is part of the Airborne Subscale Transport Aircraft Research (AirSTAR) system at the NASA Langley Research Center [9], [10]. In particular, the study addresses the application of the PSI method for the construction of the feasible solution set and for the subsequent improvement of a nominal prototype design. The paper demonstrates that the consistent application of the systematic design guidelines of $\mathcal{L}_1$ adaptive control becomes particularly beneficial for the construction of the feasible solution set. In fact, the ability to

systematically adjust the control parameters in $\mathcal{L}_1$ adaptive architectures considerably simplifies the identification of a nominal feasible solution from which to start the search for other feasible solutions and the subsequent extension of the feasible solution set. The availability of an initial feasible solution may narrow the design variable space over which the search for feasible solutions should be performed, and as a consequence, the number of Monte-Carlo trials required for the construction of the feasible set may be significantly reduced. The paper also illustrates the suitability of the PSI method (and the MOVI software package) as a tool for formulating and solving multi-criteria optimization problems for design of adaptive flight control systems. We note that the results included in this study have been produced by the MOVI software package and are based on the full nonlinear simulation of the subscale GTM AirSTAR flight test vehicle.

The paper is organized as follows. Section II provides an overview of the NASA AirSTAR facility and the $\mathcal{L}_1$ flight control law developed for the GTM aircraft; in addition, we present the nominal prototype design, with its main performance and robustness properties. Section III formulates the FCS design optimization problem, and provides a brief discussion of the PSI method and the workflow of the optimization process. The design optimization of the $\mathcal{L}_1$ FCS for the GTM aircraft is addressed in Section IV. In particular, this section provides a detailed discussion of the different steps of the optimization process, including the construction of the feasible solution set as well as the improvement of the prototype design. Finally, Section V summarizes the key results and contains the main conclusions.

II.NASA AirSTAR and $\mathcal{L}_1$ Flight Control Law

II.A. AirSTAR Facility

During 2007-2010, the NASA Aviation Safety Program created the Integrated Resilient Aircraft Control (IRAC) Project with its primary objectives to advance and transition adaptive flight control technologies as a means of increasing aviation safety. The IRAC Project had special interest in piloted flight under adverse flight conditions such as unusual attitudes, control surface failures, icing, and structural damage. As part of the project, NASA developed AirSTAR, a state-of-the-art facility designed for the purpose of investigating

and validating high-payoff technologies aimed at the loss-of-control problem using remotely-piloted subscale models without excessive risk [9], [10]. The current primary flight test vehicle of AirSTAR is the Generic Transport Model (GTM) tail number T2, which is shown in Fig. 1. The T2 is a twin-engine jet-powered and dynamically-scaled (5.5%) civil transport aircraft that was designed and instrumented to perform control law evaluation, experiment design and modeling research, in-flight failure emulation, and flight in upset conditions.

Figure 1. GTM AirSTAR unmanned aircraft and its full-scale prototype.

The AirSTAR facility also incorporates a high-fidelity nonlinear simulation of the GTM aircraft. The GTM vehicle has been extensively tested in the NASA Langley wind tunnels with particular emphasis on modeling nonlinear regions of the extended flight envelope well beyond nominal flight as well as developing a database for a number of structural damage scenarios [11],[12]. With this capability, AirSTAR provides a common research environment between simulation and flight. In this paper, we take advantage of the high-fidelity nonlinear model for the design of the $\mathcal{L}_1$ flight control law.

II.B. $\mathcal{L}_1$ Flight Control Law for the GTM Aircraft

The $\mathcal{L}_1$ flight control law developed for the AirSTAR flight test vehicle has as its primary objective in achieving reliable tracking for a variety of tasks with guaranteed stability and robustness in the presence of uncertain dynamics, such as changes due to rapidly varying flight conditions during standard maneuvers, and unexpected failures. All of these requirements are expected to be reached while providing Level 1FQ [13], [14] under nominal flight conditions, with a graceful degradation under significant adversity.

The $\mathcal{L}_1$ FCS designed for this application consists of a non-adaptive stability augmentation system (SAS) for pitch and roll, and a three-axes angle-of-attack (AOA, α), roll-rate (p), and angle-of-sideslip (AOSS, β) adaptive control augmentation system (CAS). The $\mathcal{L}_1$ adaptive controller provides thus command-tracking capabilities in both nominal and off-nominal conditions as there is no non-adaptive CAS baseline to assist it. The $\mathcal{L}_1$ CAS consists of two decoupled $\mathcal{L}_1$ controllers, one for the longitudinal channel, and another one for control of the lateral-directional dynamics. The longitudinal $\mathcal{L}_1$ controller is implemented as a Single-Input Single-Output system, and uses feedback in AOA and pitch rate to generate an elevator control signal in order to track AOA reference signals. The lateral/directional $\mathcal{L}_1$ controller is a Multiple-Input Multiple-Output architecture, and uses feedback in AOSS, roll rate, and yaw rate to generate aileron and rudder commands in order to track sideslip-angle and roll-rate reference signals with reduced coupling. In the current $\mathcal{L}_1$ FCS, the pilot adjusts directly the thrust level using the throttle lever. The reader is referred to [15–17] for a more detailed explanation of the $\mathcal{L}_1$ FCS implemented on the NASA AirSTAR flight test vehicle.

The design of the longitudinal $\mathcal{L}_1$ FCS is based on the linearized short-period dynamics of the GTM at the reference flight condition (80 kt, 1000 ft). Since the airplane is Level 1 FQ at this flight condition, the desired dynamics of the *state predictor* are chosen to be close to those of the actual aircraft. For the nominal prototype design, the natural frequency of the poles of the system is reduced from $6 rad/\sec$ to $5.5 rad/\sec$, while the damping ratio is increased from 0.47 to 0.85. A first-order low-pass filter with

DC gain 1 and a bandwidth of $20\,rad/\sec$ was used in the matched contribution to the elevator command, while two cascaded first-order low-pass filters were used in the unmatched channel, both having DC gain equal to 1 and bandwidths of $5\,rad/\sec$ and $7\,rad/\sec$ respectively. Finally, the adaptation sampling time was set to 600Hz, which corresponds to the fastest integration cycle allowed in the AirSTAR flight control computer. A first-order prefilter with $20\,rad/\sec$ of bandwidth was added to shape the pilot command. The $\mathcal{L}_1$ FCS, with its main elements as well as the design variables, is represented in Fig. 2. This *prototype* design of the state predictor, the low-pass filters, the adaptation sampling rate, and the prefilter, delivers an AOA response similar to the desired one (α_{des}); see Fig. 3. This nominal design ensures a time-delay margin of the inner-loop of approximately 85 *msec* and a gain margin of 7.2 *dB*, in wings-level flight at the reference flight condition. At this flight condition, the FQ are predicted to be Level 1 and the FCS design has no predicted pilot-induced oscillations (PIO) tendencies (for an acquisition time of 1.5 *sec*). Naturally, these metrics correspond to specific performance criteria, and these initial nominal values will be used as reference values for the definition of the criteria constraints during the optimization process.

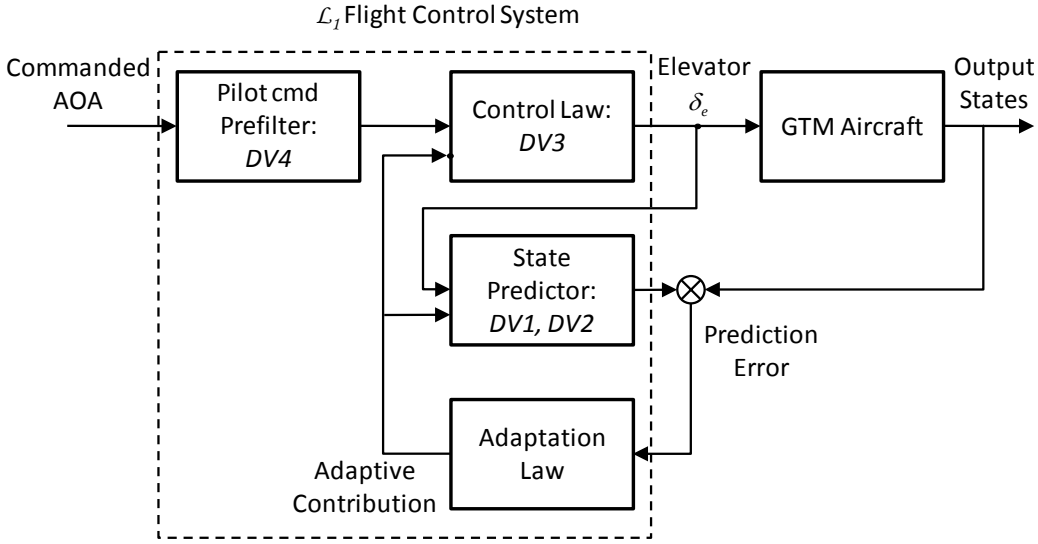

Figure 2. Longitudinal channel of the $\mathcal{L}_1$ flight control architecture.

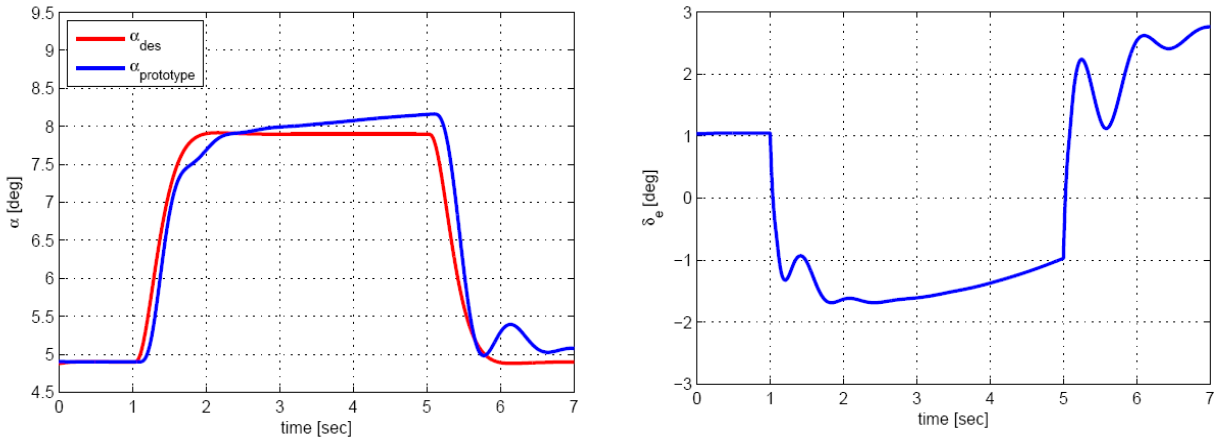

(a) Angle of attack, α

(b) Elevator deflection, δ_e

Figure 3. Prototype Design. 3 deg-AOA step response for the nominal prototype design

Next we outline the key steps of the application of the PSI method for the design optimization of the $\mathcal{L}_1$ FCS for the NASA GTM aircraft. In particular, the objective of the optimization task is to minimize the difference between the desired and actual responses, while ensuring satisfactory FQ, desired robustness margins, and reasonable actuator activity. The optimization methodology proposed in this work contains two steps. First, taking the prototype solution as a reference design, the PSI method is used for the construction of the *feasible solution set* and for determining a direction of improvement for the design of the FCS. This first step is based on a reduced and relaxed set of criteria and constraints. Then, at a second stage, the PSI method is again used to determine an *optimal design* that satisfies an extended set of performance and robustness constraints and improves the initial reference prototype.

We note that, although both the PSI and the software package MOVI have been developed to address problems with high dimensionality of both the design and the criteria spaces, for the sake of clarity, we keep the design problem within a reasonable complexity. Thus, the design procedure is only applied to the design of the longitudinal channel. Finally, we also note that all of the results included in this study are obtained by the MOVI software package combined with the MatLab environment [18], and are based on

the full nonlinear simulation model of the two-engine-powered dynamically-scaled GTM AirSTAR system, which was released by NASA in December 2009.

III. Formulation of the Optimization Problem

This section presents the formulation of the $\mathcal{L}_1$ FCS design optimization problem, indicating the sets of design variables and criteria considered in the study, as well as the criteria constraints to be satisfied.

III.A. Design Variables and Criteria

Design Variables

Since the primary objective is to improve the FQ of the prototype design while guaranteeing satisfactory robustness margins, we include the natural frequency and the damping ratio of the eigenvalues of the state-predictor dynamics (which can speed up or slow down the response of the augmented aircraft), and the bandwidth of the low-pass filter in the matched channel (which can be used to adjust the time-delay margin of the inner-loop) as design variables (*DV*); see Fig. 2. Furthermore, we also consider the optimization of the bandwidth of the pilot-command prefilter, which can be used to shape the pilot command as to prevent elevator rate limiting and avoid structural mode-flight interaction. The following list summarizes the set of optimization parameters that define the design variable space:

- *DV1. Natural frequency of the state-predictor eigenvalues* (*rad/sec*)
- *DV2. Damping ratio of the state-predictor eigenvalues (dimensionless)*
- *DV3. Bandwidth of the "matched" low-pass filter* (*rad/sec*)
- *DV4. Bandwidth of the pilot-command prefilter* (*rad/sec*)

Criteria and Pseudo-Criteria

The set of design criteria considered in this study is chosen to evaluate performance and robustness properties of the GTM aircraft augmented with the $\mathcal{L}_1$ FCS. To provide an adequate assessment of the performance characteristics and FQ of the $\mathcal{L}_1$-augmented aircraft, both pilot-off-the-loop and pilot-in-the-

loop performance metrics are included in the design procedure. The metrics considered can thus be classified in three categories:

(i) *Pilot-off-the-loop performance metrics;*

(ii) *Robustness metrics;*

(iii) *Flying qualities and PIO metrics.*

Because the present material addresses only the design of the longitudinal channel of the $\mathcal{L}_1$ FCS, the set of metrics used in this study are mainly based on the (time-domain) longitudinal response of the GTM with the $\mathcal{L}_1$ FCS closing the inner-loop. We note that some of the metrics used in this study were also proposed in [19] for the evaluation of aircraft augmented with an adaptive FCS.

Pilot-off-the-Loop Performance Metrics. This first set of metrics evaluates the performance of the augmented aircraft by characterizing its response to step inputs. In particular, the pilot-off-the-loop performance metrics are based on the time-domain response to a step command of 3 *deg* held for 4 *sec* in AOA (see Fig. 3), starting from a wings-level flight condition. The metrics capture the deviation of the actual response of the aircraft from a given desired response, which is defined to provide satisfactory flying qualities without reaching the physical limits of the platform, as well as different measures of control activity, load factor, and cross-coupling. We note that, in this study, all metrics are normalized to the amplitude of the step command considered (3 *deg*).

Next we provide a description of the metrics included in the study. First, however, we need to introduce key notations to facilitate the definition of these metrics. Along with the previously defined AOA (α) and AOA desired response (α_{des}), α_{cmd} is used here to denote the angle-of-attack pilot command; β_{des} is the AOSS desired response; p_{des} is the roll-rate desired response; A_z is the vertical acceleration; while δ_e is the elevator deflection command. We let t_0 be the time instant at which the step command is applied, and define t_f as the final time instance considered for the performance evaluation ($t_f = t_0 + 4$ *sec*). With the above notations, the metrics are formally defined as follows:

P1. Final deviation: this metric captures the final deviation of the actual AOA response from the desired AOA response at 4 *sec* after the application of the step command. This metric is set to zero if the actual response reaches the AOA reference command before the end of the 4-second step:

$$P1 = \begin{cases} \left|\alpha(t_f) - \alpha_{des}(t_f)\right| & \text{if } \alpha(t) < \alpha_{cmd}, \forall t \in [t_0, t_f] \\ 0 & \text{otherwise} \end{cases}$$

This metric penalizes or excludes sluggish responses.

P2. Maximum deviation from desired AOA response: this metric captures the maximum deviation (in absolute value) of the actual AOA response from the desired AOA response:

$$P2 = \max_{t \in [t_0, t_f]} \left|\alpha(t) - \alpha_{des}(t)\right|$$

P3. Integral deviation from desired AOA response: this metric is defined as the (truncated) $\mathcal{L}_2$-norm of the deviation of the actual AOA response from the desired AOA response:

$$P3 = \int_{t_0}^{t_f} \left|\alpha(t) - \alpha_{des}(t)\right| dt$$

P4. Overshoot in AOA response: this metric captures possible overshoots and low-damping characteristics in the AOA response:

$$P4 = \begin{cases} \max_{t \in [t_0, t_f]} \left|\alpha(t)\right| & \text{if } \alpha(t) > \alpha_{cmd}, \text{for some } t \in [t_0, t_f] \\ \alpha_{cmd} & \text{otherwise} \end{cases}$$

P5. Maximum deviation from desired AOA rate response: this metric captures the maximum rate deviation (in absolute value) of the actual AOA response from the desired AOA response:

$$P5 = \max_{t \in [t_0, t_f]} \left|\dot{\alpha}(t) - \dot{\alpha}_{des}(t)\right|$$

P6. Integral deviation from desired AOA rate response: this metric is defined as the (truncated) $\mathcal{L}_2$-norm of the rate deviation of the actual AOA response from the desired AOA response:

$$P6 = \int_{t_0}^{t_f} \left| \dot{\alpha}(t) - \dot{\alpha}_{des}(t) \right| dt$$

The metrics *P1* to *P6* provide a good characterization of the transient response of the augmented aircraft when compared to a given desired response. Next, we present a set of metrics that can be extracted from the same step response and complement the AOA metrics defined above.

P7. *Maximum vertical acceleration:* load factor (and passenger comfort) requirements can be captured by the maximum vertical acceleration during the step response:

$$P7 = \max_{t \in [t_0, t_f]} \left| A_z(t) \right|$$

P8. *Control effort:* this metric is defined as the (truncated) $\mathcal{L}_2$-norm of the elevator deflection command:

$$P8 = \int_{t_0}^{t_f} \left| \delta_e(t) \right| dt$$

This metric penalizes the flight control designs that require a high control activity to achieve a desired control objective. It is important to note, however, that a high control effort might just be the result of a faster AOA response, and therefore a large *P8* might not always be an undesirable response characteristic.

P9. *Maximum elevator rate:* excessive control rate can be identified by the following metric:

$$P9 = \max_{t \in [t_0, t_f]} \left| \dot{\delta}_e(t) \right|$$

This metric penalizes designs with high elevator rates in order to prevent undesirable effects from rate limiting.

P10. *Maximum elevator acceleration:* high-order derivatives of the control commands are coupled to the flexible modes of the aircraft. The following metric, based on the second derivative of the elevator command, captures excessive accelerations and oscillations in the control command that could potentially lead to unwanted structural mode interactions:

$$P10 = \max_{t\in[t_0,t_f]} \left|\ddot{\delta}_e(t)\right|$$

P11. Maximum of $\mathcal{L}_1$ prediction error: this metric captures the maximum error between the actual system state and the state of the $\mathcal{L}_1$ state predictor, usually denoted by $\tilde{x}(t)$:

$$P11 = \max_{t\in[t_0,t_f]} \left\|\tilde{x}(t)\right\|_\infty$$

In $\mathcal{L}_1$ adaptive control architectures, the accurate estimation of system uncertainties and the performance guarantees rely on the (small) "size" of the prediction error $\tilde{x}(t)$. This metric is used to monitor the correct functioning of the $\mathcal{L}_1$ adaptive controller.

P12. Maximum deviation in cross-coupling dynamics: this metric captures the lateral-directional coupling induced by a command in the longitudinal channel:

$$P12 = \max_{t\in[t_0,t_f]} \left|\delta_e(t)\right|((\beta(t)-\beta_{des}(t))^2 + (p(t)-p_{des}(t))^2)$$

This metric primarily provides valuable information for the design of the lateral-directional FCS.

P13. Integral deviation in cross-coupling dynamics: this metric is the integral version of the previous cross-coupling metric and is defined as follows:

$$P13 = \int_{t_0}^{t_f} \left|\delta_e(t)\right|((\beta(t)-\beta_{des}(t))^2 + (p(t)-p_{des}(t))^2)dt$$

Similar to *P12*, this metric would be more adequate for the design of the lateral-directional control system, and both are included in this study only to illustrate a set of additional metrics that can be derived from the response of the augmented aircraft to a command in the longitudinal channel.

Robustness Margins. In this preliminary study, the only robustness metric considered for optimization is the *time-delay margin* of the closed-loop adaptive system. It is defined at the input of the aircraft (time

delay inserted at the elevator deflection command), and it is derived from the time-domain response of the augmented aircraft. For a given wings-level flight condition and with the pilot-off-the-loop, a small perturbation in the trim (initial) condition is introduced. The time-delay margin is determined as the minimum time delay that produces sustained oscillations in the AOA response as the $\mathcal{L}_1$ FCS tries to stabilize the aircraft at the given trim condition. In this study, this robustness metric will be denoted by *R1*. Note that the time delay introduced in the elevator control channel is in addition to the 25 *msec* that is already modeled in the AirSTAR simulation environment.

Criteria addressing FQ and PIO characteristics. Finally, predictions for both FQ and PIO tendencies have also been included in order to complement the pilot-off-the-loop performance metrics presented above. For this study, we consider the Time-Domain Neal-Smith (TDNS) FQ and PIO criteria, which was specifically developed for nonlinear aircraft dynamics and nonlinear FCS. For a detailed description of this criterion, the reader is referred to [20]. The reader can also find in [21] a study on the prediction of flying qualities and adverse pilot interactions in the GTM augmented with the $\mathcal{L}_1$ FCS. We use four different metrics, extracting all of them from the TDNS criterion for an acquisition time of 1.5 *sec*, to characterize the FQ and PIO tendencies of the augmented aircraft:

FQ1. *Tracking performance:* In the TDNS criterion, the root-mean-squared tracking error is used to evaluate the closed-loop performance with the pilot-in-the-loop. A value of zero means that the pilot is able to perfectly track (with zero error) the reference command after the specified acquisition time.

FQ2. *Pilot workload:* In the TDNS criterion, the pilot workload is given by the pilot compensation phase angle (in degrees), which is derived from the optimal pilot model obtained from the criterion. A value of zero means that there is no need for either pilot lead or lag compensation.

FQ3. *FQ level:* The two metrics above, *FQ1* and *FQ2*, are used to determine the predicted FQ level based on the FQ boundaries proposed in the criterion. *FQ3* is a discrete metric, and it only admits the values 1, 2, and 3, which correspond to Level 1, Level 2, and Level 3 FQ, respectively.

FQ4. *PIO tendency:* The TDNS criterion also provides a prediction for the susceptibility of the augmented aircraft to PIO. This PIO-susceptibility metric is used to complement the flying qualities metrics

discussed above. According to the TDNS criterion, a value above 100 implies that the augmented aircraft is PIO-prone, whereas a value below 100 indicates a PIO-immune configuration.

The set of metrics described above will be used is used in Section IV to improve a prototype design of the longitudinal channel of the $\mathcal{L}_1$ FCS. For the first stage of the design –extension of the feasibility set–, only a subset of these metrics will be used. The full set of metrics will be used in the second stage to optimize the design of the adaptive control system. Based on the objectives of the task and previous flight control design expertise, the following vectors of criteria {*P1, P2, P3, P4, P5, P6, FQ1, FQ2, FQ3, FQ4, R1*} and pseudo-criteria {*P7, P8, P9, P10, P11, P12, P13*} are defined.

III.B. Criteria Constraints

Based on the metrics defined, the final design of the $\mathcal{L}_1$ FCS should *ideally* verify the set of control objectives at the reference flight condition of 80 kt of (equivalent) airspeed and 1000 ft of altitude. Corresponding to this flight conditions a set of three criteria constraints were defined a priory:

$$P1 \leq 0.1,\ FQ3 = 1,\ \text{and}\ P4 \leq 1.2.$$

The first and second conditions address directly the control specifications, namely the final value of the step response within 10% of the desired, and the predicted Level 1 FQ. The third inequality imposes a 20% constraint on the overshoot in the step response, establishing thus a (loose) bound on the acceptable transient performance characteristics of the actual AOA response. Due to significant difficulty of defining all criteria constraints consistent with feasibility of the solution, the rest of the constraints will be identified interactively while analyzing the test tables.

IV. Solutions and Analysis

This section presents the two steps of iterative application of the PSI method to the design improvement of the longitudinal channel of the $\mathcal{L}_1$ FCS. As mentioned earlier, the first iteration uses a reduced set of the control metrics. Numerical implementation of this first step is relatively efficient with the “computational price” of one solution measured in minutes. At the second step, when using the extended set of criteria, the

efficiency of numerical implementation becomes critical because the "computational price" of one solution is measured in tenth of minutes.

As it was mentioned above the PSI method does not alter the optimization task by "mapping" a set of multiple criteria to just one scalar functional. To support this multi-criteria approach, the MOVI package provides a rich set of analysis tools. Besides numerical results organized as a test table, it provides a number of visual tools. In particular, histograms of design variables, criterion versus design variable plots, and the criterion versus criterion plots are the most intuitive and effective tools used during the interactive analysis. A comprehensive introduction to the effective use of the MOVI package can be found in [6], [7].

IV.A. First iteration: Construction of the Feasible Solution Set

The construction the feasible solution set starts by defining test intervals for the design variables. These test intervals have been identified with respect to the nominal prototype solution obtained from the $\mathcal{L}_1$ design procedure (see Table 1).

Table 1. Initial intervals of design variables

Design variable	$\mathcal{L}_1$ Prototype	Initial intervals of variation of design variables	
		min	max
DV1	5.50E+00	4.00E+00	8.00E+00
DV2	8.50E-01	5.00E-01	1.10E+00
DV3	2.00E+01	5.00E+00	3.00E+01
DV4	2.00E+01	1.00E+01	5.00E+01

The objective of the first step is to find a direction of improvement for the nominal design. More precisely, we aim here at determining tight intervals for the design variables characterizing the state predictor (*DV1* and *DV2*) that would provide Level 1 FQ and would not deviate from the desired response

defined previously. To this end, the design is to be minimized with respect to the following reduced number of criteria {*P1, P2, P3, P4, P5, P6, FQ1, FQ2*}.

The robustness metric *R1* and the PIO metric *FQ4* are not included in this first step because their evaluation is computationally expensive; these metrics will be considered in the next step of the optimization process when the domain of the design variables becomes significantly refined. The metrics *P7* through *P10* are not included in the set of criteria because improved flying qualities may require "high" values of these metrics. Nevertheless, they are included in the optimization process as pseudo-criteria[7] thus providing useful inside onto the dynamics of the augmented aircraft. Similarly, the metric *P11*, which can be used to monitor the correct operation of the $\mathcal{L}_1$ adaptive controller, does not need to be minimized as long as it remains a couple of orders of magnitude below the system state (truncated) $\mathcal{L}_\infty$-norm. Finally, the metrics *P12* and *P13* are included for the sake of completeness and should be considered only for the design of the lateral-directional control system.

The MOVI package performs a predefined set of numerical trials and then forms a test table. Interactive work with the test table consists of sequential tightening of the DV constraints and is well supported by a number of graphical instruments implemented in MOVI. The final results achieved in this first iteration of the optimization process, is based on 1024 tests. Out of these 1024 tests, 427 vectors did not satisfy the a priori given criteria constraints. The solutions that did not satisfy the constraints entered the *table of criteria failures;* every entry of this table is available for a detailed analysis. The remaining 597 vectors which did satisfy a priori given criteria constraints were used to construct the test table. While tightening the criteria constraints in the test table, the following new criteria constraints were formulated, see Table 2. Note, that while analyzing the test table, the constraint of *P4* was significantly tightened to the value of 1.02. Furthermore, the response on criteria *P1* is not presented in the table because all solutions provided identical response, *P1*=0. Only 20 solutions were found to be feasible according to these criteria constraints, all of them contributing to the Pareto optimal solutions. A fragment of the criteria table is given in Table 3.

[7] Pseudo-criterion differs from a criterion by the fact that it is not included in the calculation of the Pareto front, for more details see [6].

Table 2. Criteria constraints

$P2 \leq 0.2$	(min)	$P9 \leq 15$	(pseudo)
$P3 \leq 0.2$	(min)	$P10 \leq 300$	(pseudo)
$P4 \leq 1.02$	(min)	$P11 \leq 0.25$	(pseudo)
$P5 \leq 1$	(min)	$P12 \leq 0.01$	(pseudo)
$P6 \leq 0.3$	(min)	$P13 \leq 0.01$	(pseudo)
$P7 \leq 0.25$	(pseudo)	$FQ1 \leq 0.1$	(min)
$P8 \leq 5$	(pseudo)	$FQ2 \leq 45$	(min)

Table 3. Fragment of Criteria Table

Criteria		Prototype	Pareto optimal solutions						
			#241	#281	#329	#409	#649	#825	#993
P2	(min)	1.30E-01	1.04E-01	8.40E-02	9.14E-02	8.97E-02	6.03E-02	7.44E-02	5.39E-02
P3	(min)	1.54E-01	1.16E-01	1.03E-01	1.06E-01	1.04E-01	8.72E-02	9.51E-02	8.84E-02
P4	(min)	1.0E+00	1.00E+00	1.00E+00	1.00E+00	1.00E+00	1.01E+00	1.00E+00	1.00E+00
P5	(min)	3.15E-01	5.37E-01	9.36E-01	9.68E-01	6.29E-01	8.63E-01	8.58E-01	6.89E-01
P6	(min)	1.49E-01	1.97E-01	2.21E-01	2.58E-01	2.03E-01	1.74E-01	1.94E-01	1.32E-01
P7	(pseudo)	1.51E-01	1.65E-01	1.74E-01	1.84E-01	1.72E-01	1.83E-01	1.78E-01	1.75E-01
P8	(pseudo)	3.24E+00	3.3E+00	3.29E+00	3.31E+00	3.30E+00	3.31E+00	3.30E+00	3.31E+00
P9	(pseudo)	5.96E+00	1.17E+01	7.55E+00	9.1E+00	1.09E+01	1.11E+01	9.36E+00	1.16E+01
P10	(pseudo)	1.07E+02	2.42E+02	1.34E+02	1.72E+02	2.16E+02	2.24E+02	1.76E+02	2.44E+02
P11	(pseudo)	7.45E-02	7.79E-02	6.02E-02	6.82E-02	8.10E-02	7.72E-02	7.22E-02	7.77E-02
P12	(pseudo)	1.01E-04	1.84E-04	1.87E-04	2.08E-04	2.06E-04	2.29E-04	2.14E-04	2.09E-04
P13	(pseudo)	3.16E-05	6.18E-05	6.87E-05	8.01E-05	7.00E-05	8.18E-05	7.58E-05	7.03E-05
FQ1	(min)	1.23E-02	6.73E-02	9.29E-02	9.74E-02	6.86E-02	9.05E-02	7.80E-02	8.85E-02
FQ2	(min)	5.36E+01	4.42E+01	4.35E+01	4.03E+01	4.22E+01	3.79E+01	4.10E+01	4.00E+01

Analysis of the criteria table shows that solution #993 is the most preferable one. This solution is equivalent to others with respect to criterion *P4*, it is superior to others over a set of 5 criteria {*P2, P3, P6,*

FQ1, FQ2} and is weaker than the prototype only with respect to the criterion *P5*. Furthermore, the other 19 solutions are better than the prototype with respect to four criteria {*P2, P3, FQ1, FQ2*}. However, none of the solutions are superior to the prototype with respect to criterion *P5*. In particular, this observation implies that, if the prototype design vector had been sampled by the system, then it would belong to the Pareto set. On the other hand, this result confirms that the solution obtained following the basic $\mathcal{L}_1$ design guidelines are near optimal.

This analysis allows defining the direction of further search. In particular, the results provide tight intervals for the design variables *DV1* and *DV2* characterizing the state-predictor dynamics, and expose the necessity of extending the initial intervals of variation of the design variables *DV3* and *DV4;* see for example Fig. 4. Based on these results and their analysis, a new experiment is carried out to, first, improve the feasible solution set and, second, determine an optimal solution of the $\mathcal{L}_1$ FCS design that improves the prototype with respect to an extended set of criteria.

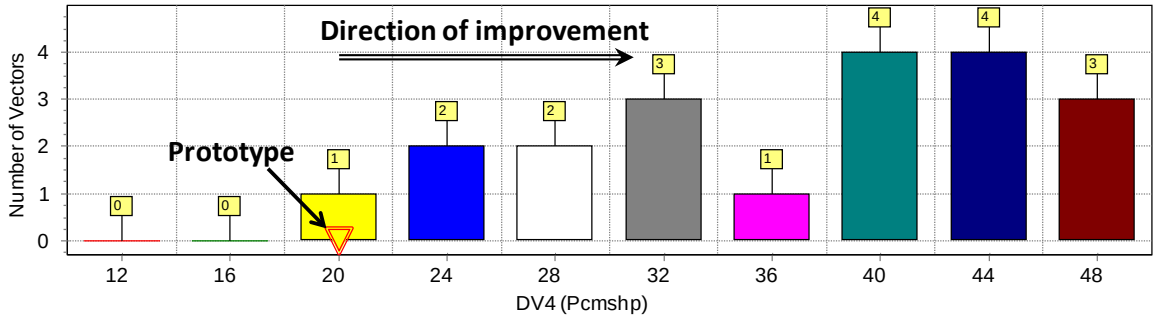

Figure 4. A histogram of *DV4* distribution along with the prototype solution and the direction of improvement.

IV.B. Second iteration: Design Improvement

Based on the analysis of the histograms and criteria table just presented, we adjust the intervals of variation of the design variables as given in Table 4.

Table 4. Refined intervals of design variables

Design variable	Prototype	Initial intervals of variation of design variables

		min	max
DV1	5.50E+00	5.50E+00	7.00E+00
DV2	8.50E-01	6.50E-01	0.90E+00
DV3	2.00E+01	9.80E+00	4.00E+01
DV4	2.00E+01	1.80E+01	6.50E+01

The criteria constraints remain unchanged, whereas the design is now to be optimized with respect to the extended set of criteria {*P2*, *P3*, *P4*, *P5*, *P6*, *FQ1*, *FQ2*, *FQ4*, *R1*}. All of these criteria are to be minimized except for *R1*, which is to be maximized.

The results of second iteration are based on 512 tests producing 124 feasible solutions. All these solutions are Pareto optimal. The histograms in this second iteration have stronger distributions of the feasible solutions than in the first iteration. Figure 5a represents the distribution of 124 solutions for *DV1*.

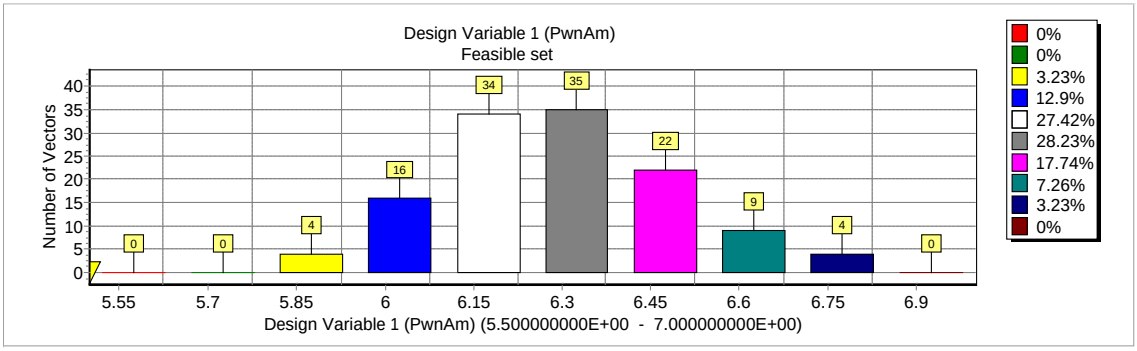

(a) Original criteria constraints

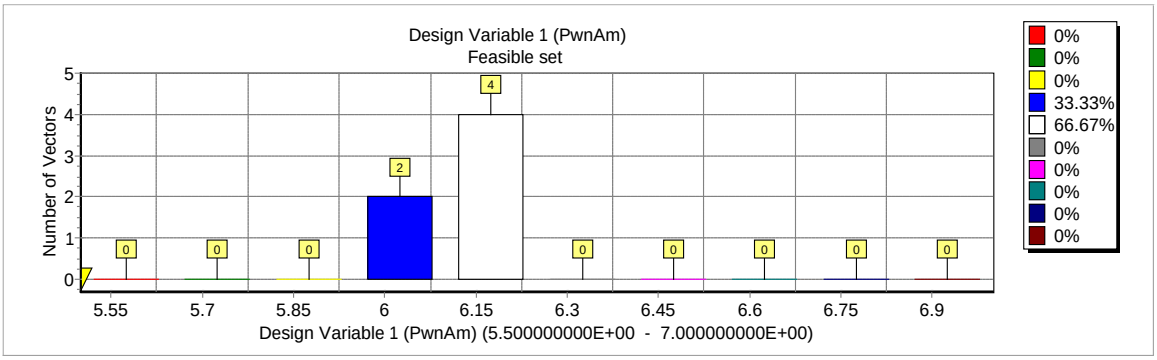

(b) Tightened criteria constraints

Figure 5. PSI Iteration 2. Distribution of feasible solutions of DV1 with the original (top) and with tightened criteria constraints (bottom).

As a result, analysis of the test table and histograms leads to a stronger set of criteria and pseudo-criteria constraints, presented in Table 5. According to these new constraints, only 6 solutions are feasible, and all of them are Pareto optimal. The values of the design variables and criteria of the Pareto optimal solutions are given in Tables 6 and 7, respectively. The new distribution of the feasible solutions for these criteria and pseudo-criteria constraints is significantly tighter; see Fig. 5. The new histograms clearly identify tight intervals for all of the design variables in which the optimal solutions lie.

Table 5. Second iteration, refined criteria constraints

$P2 \leq 0.1$	(min)	$P10 \leq 200$	(pseudo)
$P3 \leq 0.15$	(min)	$P11 \leq 0.1$	(pseudo)
$P4 \leq 1.02$	(min)	$P12 \leq 0.01$	(pseudo)
$P5 \leq 1$	(min)	$P1\ 3 \leq 0.01$	(pseudo)
$P6 \leq 0.25$	(min)	$FQ1 \leq 0.1$	(min)
$P7 \leq 0.2$	(pseudo)	$FQ2 \leq 45$	(min)
$P8 \leq 5$	(pseudo)	$FQ4 \leq 5$	(min)
$P9 \leq 10$	(pseudo)	$R1 \geq 80$	(max)

Table 6. Second iteration. Table of design variables

Design variable	Prototype	#993, First Iteration	Pareto optimal solutions					
			#106	#202	#254	#318	#358	#462
DV1	5.50E+00	6.12E+00	6.00E+00	5.99E+00	6.24E+00	6.23E+00	6.10E+00	6.18E+00
DV2	8.50E+00	7.09E-01	7.34E-01	7.49E-01	7.76E-01	7.33E-01	7.81E-01	7.18E-01
DV3	2.0E+01	2.70E+01	2.52E+01	1.67E+01	1.81E+01	2.18E+01	1.69E+01	1.58E+01
DV4	2.0E+01	4.93E+01	3.16E+01	3.20E+01	2.10E+01	2.72E+01	2.57E+01	3.11E+01

Table 7. Second iteration. Table of criteria

Criteria		Prototype	Pareto optimal solutions					
			#106	#202	#254	#318	#358	#462
P2	(min)	1.30E-001	6.01E-01	8.45E-02	9.17E-02	7.04E-02	9.63E-02	8.28E-02
P3	(min)	1.54E-01	9.60E-02	1.13E-01	1.11E-01	9.66E-02	1.18E-01	1.04E-01
P4	(min)	1.0E+00	1.00E+00	1.00E+00	1.00E+00	1.00E+00	1.01E+00	1.00E+00
P5	(min)	3.15E-01	6.13E-01	6.81E-01	8.85E-01	8.43E-01	7.71E-01	8.63E-01
P6	(min)	1.49E-01	1.28E-01	1.67E-01	2.16E-01	1.78E-01	1.94E-01	2.11E-01
P7	(pseudo)	1.51E-01	1.68E-01	1.67E-01	1.72E-01	1.76E-01	1.68E-01	1.78E-01
P8	(pseudo)	3.24E+00	3.29E+00	3.29E+00	3.29E+00	3.30E+00	3.29E+00	3.31E+00
P9	(pseudo)	5.96E+00	9.09E+00	9.1E+00	7.9E+00	9.05E+00	8.43E+00	9.54E+00
P10	(pseudo)	1.07E+02	1.77E+02	1.78E+02	1.43E+02	1.72E+02	1.59E+02	1.85E+02
P11	(pseudo)	7.45E-02	6.62E-02	6.60E-02	6.09E-02	6.74E-02	6.31E-02	6.95E-02
P12	(pseudo)	1.01E-04	1.81E-04	1.70E-04	1.80E-04	2.01E-04	1.69E-04	1.98E-04
P13	(pseudo)	3.16E-05	6.02E-05	5.89E-05	6.58E-05	7.13E-05	6.01E-05	7.27E-05
FQ1	(min)	1.23E-02	9.93E-02	9.81E-02	9.34E-02	9.26E-02	9.20E-02	9.64E-02
FQ2	(min)	5.36E+01	4.33E+01	4.41E+01	4.38E+01	4.14E+01	4.46E+01	4.10E+01
FQ4	(min)	4.68E+00	4.08E+00	4.19E+00	3.87E+00	3.88E+00	3.84E+00	3.97E+00
R1	(max)	8.50E+01	8.50E+01	1.05E+02	8.00E+01	8.50E+01	9.00E+01	1.00E+02

Further analysis of Table 7 shows that all solutions of second iteration, as well as the #993 from the first iteration, belong to the very tight intervals of the first and second design variables. The first three parameters (*DV1* to *DV3*) of #993 and #106 are almost identical. However, one can see that #993, while providing good response of many criteria, does not satisfy the new constraints on criteria *P9* and *P10* (elevator workload). Moreover, #993 also fails to satisfy the constraint on the criteria *FQ3*.

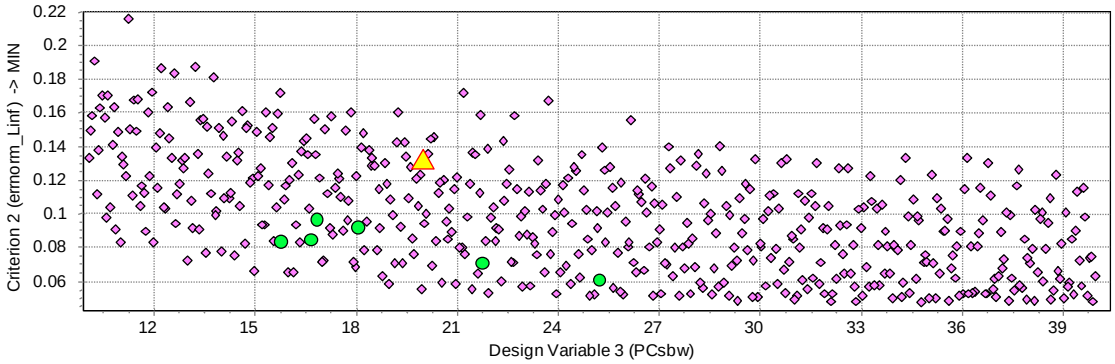

(a) Criterion *P2* (max AOA deviation) vs. design variable *DV3*.

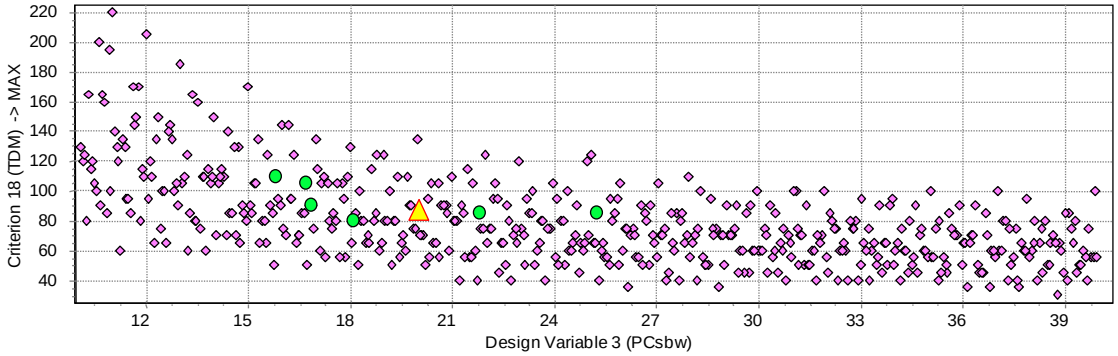

(b) Criterion *R1* (time delay margin) vs. design variable *DV3*

Figure 6. PSI Iteration 2. Dependencies of criteria *P2* and *R1* on the design variable *DV3*.

The analysis of the test tables, dependencies of criteria on design variables, and dependencies between criteria, allows determining the most preferable solutions. In particular:

- Figure 6 shows the influence of the bandwidth of the "matched" low-pass filter (*DV3*) on the (pilot-off-the-loop) tradeoff between performance criterion *P2* (*P3* shows the same trend) and robustness (*R1*) of the augmented aircraft. From this observation we conclude that criteria *P2* (*P3*) and *R1* are contradictory with respect to the design variable *DV3*. This means that improvement of the tracking performance requires an increase in the bandwidth of the low-pass filter, which in turn results in degradation of the time-delay margin of the augmented aircraft. This tradeoff is consistent with the predictions of the $\mathcal{L}_1$ adaptive control theory.

- Figure 7 shows the dependencies of the flying qualities criterion *FQ1* (*FQ2* is similar) on the design variable *DV2*. While in the first PSI iteration the dependency of the criterion *FQ2* on the design variable *DV2* was not obvious, now it becomes apparent that a smaller damping ratio results in reduced (lead) pilot compensation.

The dependency of flying qualities criteria *FQ1* and *FQ2* obtained in this iteration is also similar to those obtained in the first iteration, thus demonstrating significant improvement of predicted flying qualities over the prototype design, but now in the extended criteria space.

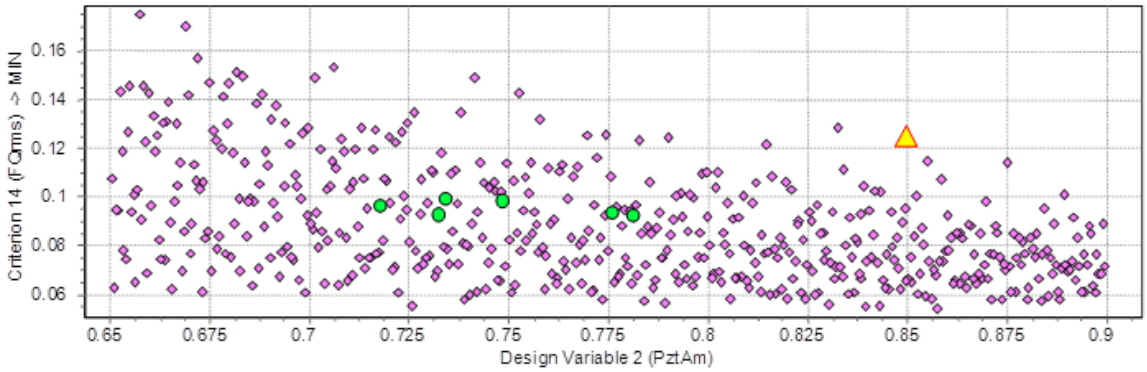

Figure 7. PSI Iteration 2. Dependencies of criteria *FQ1* (tracking performance) on the design variable *DV2*.

- Finally, Figure 8 shows the dependency between criteria *P3* and *R1*, which illustrates the fundamental tradeoff between performance and robustness of the closed-loop adaptive system with the pilot off the loop. While all of the optimal solutions reduce the deviations from the desired response with respect to the prototype design, only three of these solutions exhibit a better time-delay margin than the prototype design (#202, #462), and two exhibit a similar margin (#106, #318).

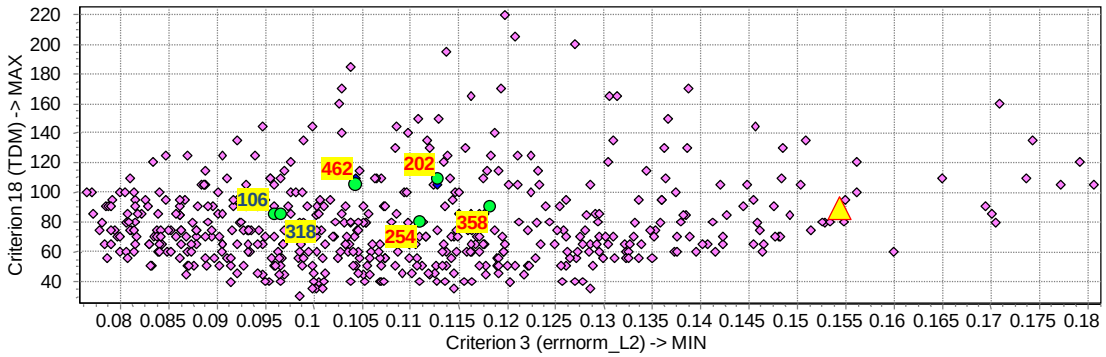

Figure 8. PSI Iteration 2. Relation between criteria *R1* (time delay margin) and *P3* (integral deviation of AOA).

As a result of iterative two-step correction of initial constraints, six Pareto optimal solutions have been found. Analysis of these solutions shows that #106, #202, #358, and #462 improved the prototype design by six criteria simultaneously. Although all 6 solutions are practically equivalent, preference is given to the design vector #202, as it provides better tradeoff between the (predicted) flying qualities (*FQ1*, *FQ2*) and the time-delay margin (*R1*), while minimizing the difference with the desired response; see Fig. 9. We notice that, when compared to the time response of the prototype design, the AOA response and the elevator workload of the *optimal* solution #202 provides a faster response (smaller rise time) with a minimal increase in the elevator workload.

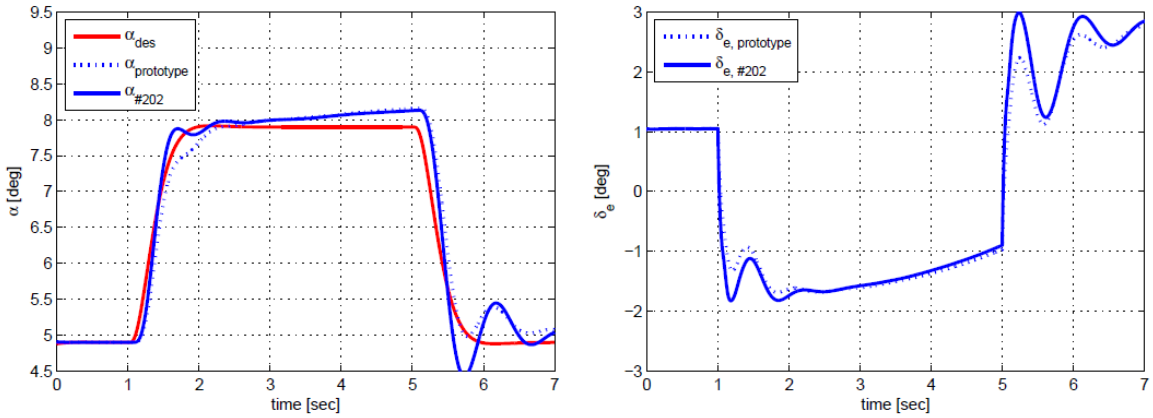

(a) Angle of attack, α

(b) Elevator deflection, δ_e

Figure 9. Optimal Design #202. 3 deg-AOA step response.

V. Conclusion.

This paper presented results of the application of the PSI method and the MOVI software package for the design optimization of the $\mathcal{L}_1$ flight control system implemented on the AirSTAR GTM aircraft. In particular, the study has addressed the construction of the feasible solution as well as the improvement of a nominal prototype design. For this purpose, we have formulated and solved an optimization problem with *4 design variables* –defining the eigenstructure of the state-predictor state matrix, the bandwidth of the low-pass filter, and the bandwidth of the pilot-command prefilter– and *18 criteria* –characterizing pilot-off-the-loop performance metrics, robustness metrics, as well as flying qualities and PIO metrics. This study demonstrates that consistent application of the systematic design guidelines of $\mathcal{L}_1$ adaptive control becomes particularly beneficial for the construction of the feasible solution set. Additionally, the results of the study are consistent with the theoretical claims of the theory of $\mathcal{L}_1$ adaptive control in terms of robustness and performance. Moreover, the developed procedure and the obtained results confirm the suitability of the PSI method for the multi-criteria optimization of an adaptive flight control law subject to desired control specifications.

Finally, we want to emphasize that the insights gained during the optimization process with the MOVI software contributed to the successful flight verification and validation [17] of the designed $\mathcal{L}_1$ adaptive control law at NASA LARC.

Acknowledgments

This work was supported by Air Force Office of Scientific Research [grant number FA9550–09–1–0265]; and NASA [grant numbers NNX08BA64A and NNX08BA65A].

Bibliography

1 Jacklin, S.A., Lowry, M.R, Schumann, J.M., Gupta, P.P., Bosworth, J.T., Zavala, E.K., Kelly, J. W., Hayhurst, K.J., Belcastro, C.M., "Verification, Validation, and Certification Challenges for Adaptive Flight-Critical Control System Software," in proceedings of *AIAA Guidance Navigation and Control Conference and Exhibit*, 2004, August, AIAA-2004-5258.

2 Wise, K.A., Lavretsky, E., and Hovakimyan, N., "Adaptive Control of Flight: Theory, Applications, and Open Problems," in proceedings of *American Control Conference*, 2006, June, Minneapolis, MN, pp. 8-10.

3 Jacklin, S. A., "Closing Certification Gaps in Adaptive Flight Control Software," in proceedings of *AIAA Guidance, Navigation and Control Conference*, Honolulu, HI, August 2008, AIAA-2008-6988.

4 Hovakimyan, N. and Cao, C., $\mathcal{L}_1$ *Adaptive Control Theory*, Society for Industrial and Applied Mathematics, Philadelphia, PA, 2010.

5 Kim, K. K. K. and Hovakimyan, N., "Development of Verification and Validation Approaches for $\mathcal{L}_1$ Adaptive Control: Multi-Criteria Optimization for Filter Design," in proceedings of *AIAA Guidance, Navigation and Control Conference*, Toronto, Canada, August 2010.

6 Statnikov, R. B., and Matusov, R. B., *Multicriteria Analysis in Engineering*. Dordrecht/Boston/London: Kluwer Academic Publishers, 2002.

7 Sobol', I. M., and Statnikov, R.B., *Selecting Optimal Parameters in Multicriteria Problems*, 2nd ed. Moscow: Drofa, 2006.

8 Statnikov, R. B., and Statnikov, A. R., "Software Package MOVI 1.4 for Windows: User's Manual, Certificate of Registration." .

9 Jordan, T. L., Langford, W. M., and Hill, J. S., "Airborne Subscale Transport Aircraft Research Testbed-Aircraft Model Development," in proceedings of *AIAA Guidance, Navigation and Control Conference*, San Francisco, CA, August 2005, AIAA-2005-6432.

10 Jordan, T. L., Foster, J. V., Bailey, R. M., and Belcastro, C. M., "AirSTAR: A UAV Platform for Flight Dynamics and Control System Testing," in proceedings of *AIAA Aerodynamic Measurement Technology and Ground Testing Conference*, San Francisco, CA, June 2006, AIAA-2006-3307.

11 Foster, J. V., Cunningham, K., Fremaux, C.M., Shah, G.H., Stewart, E.C., Rivers, R.A., Wilborn, J.E., Gato, W., "Dynamics Modeling and Simulation of Large Transport Airplanes in Upset Conditions," ," in proceedings of *AIAA Guidance, Navigation and Control Conference*, San Francisco, California, Aug. 15-18, 2005, AIAA-2005-5933.

12 Shah, G.H., "Aerodynamic Effects and Modeling of Damage to Transport Aircraft," in proceedings of *AIAA Atmospheric Flight Mechanics Conference*, Honolulu, HI, August 18-21, 2008, AIAA-2008-6203.

13 Stengel, R., *Flight Dynamics*, Princeton University Press, 2004.

14 Mil. Standard, "MIL-HDBK-1797 Flying qualities of piloted aircraft," *US Department of Defense pg*, 19 December 1997.

15 Cao, C., and Hovakimyan, N., "L1 Adaptive Controller for Multi-Input Multi-Output Systems in the Presence of Unmatched Disturbances," in proceedings of *American Control Conference*, issue: 6, IEEE, 2008, pp. 4105-4110.

16 Gregory, I. M., Cao, C., Xargay, E., Hovakimyan, N., and Zou, X., "L1 Adaptive Control Design for NASA AirSTAR Flight Test Vehicle," in proceedings of *AIAA Guidance, Navigation, and Control Conference*, Chicago, Illinois, Aug. 10-13, 2009, AIAA-2009-5738.

17 I. M. Gregory, Xargay, E., Cao, C., Hovakimyan, N., "Flight Test of an L 1 Adaptive Controller on the NASA AirSTAR Flight Test Vehicle," in proceedings of *AIAA Guidance, Navigation, and Control Conference*, Toronto, Ontario, Aug. 2-5, 2010, AIAA-2010-8015.

18 "MathWorks - MATLAB and Simulink for Technical Computing," *MathWorks*, 2011. Available Online at http://www.mathworks.com/.

19 Stepanyan, V., Krishnakumar, K., Nguyen, N., and Eykeren, N., "Stability and performance Metrics for Adaptive Flight Control," in proceedings of *AIAA Guidance, Navigation and Control Conference*, Chicago, IL, August 2009, AIAA-2009-5965.

20 Bailey, R. E. and T. J. Bidlack, "Unified Pilot-Induced Oscillation Theory. Volume IV: Time-Domain Neal-Smith Criterion," Tech. Rep. WL-TR-96-3031, Air Force Wright Laboratory, December 1995.

21 R. Choe, E. Xargay, N. Hovakimyan, and I. M. Gregory, "L 1 Adaptive Control under Anomaly Flying Qualities and Adverse Pilot Interaction," *AIAA Guidance Navigation and Control Conference 2 5 August 2010 Toronto Ontario Canada*, no. August, pp. 1-29, 2010.

Nomenclature

α	angle of attack
β	angle of sideslip
p	roll rate
A_z	vertical acceleration
δ_e	elevator deflection command
α_{cmd}	angle of attack pilot command
α_{des}	angle of attack desired response
β_{des}	side slip angle desired response
p_{des}	roll rate desired response

List of Figures

Figure 6. PSI Iteration 2. Dependencies of criteria *P2* and *R1* on the design variable *DV3.*

Figure 7. PSI Iteration 2. Dependencies of criteria *FQ1* (tracking performance) on the design variable *DV2.*

Figure 8. PSI Iteration 2. Relation between criteria *R1* (time delay margin) and *P3* (integral deviation of AOA).

Figure 9. Optimal Design #202. 3 deg-AOA step response.